Acta Oceanol. Sin., 2021, Vol. 40, No. 9, P. 43–52
https://doi.org/10.1007/s13131-021-1775-5
http://www.aosocean.com
E-mail: ocean2@hyxb.org.cn

Copper and zinc isotope variations in ferromanganese crusts and their isotopic fractionation mechanism

Lianhua He[1, 2], Jihua Liu[1, 2*], Hui Zhang[1, 2], Jingjing Gao[1, 2], Aimei Zhu[1, 2], Ying Zhang[1, 2]

[1] Key Laboratory of Marine Geology and Metallogeny, First Institute of Oceanography, Ministry of Natural Resources, Qingdao 266061, China

[2] Laboratory for Marine Geology, Pilot National Laboratory for Marine Science and Technology (Qingdao), Qingdao 266061, China

Received 2 June 2020; accepted 27 September 2020

Abstract

Ferromanganese (Fe-Mn) crusts are potential archives of the Cu and Zn isotope compositions of seawater through time. In this study, the Cu and Zn isotopes of the top surface of 28 Fe-Mn crusts and 2 Fe-Mn nodules were analysed by MC-ICP-MS using combined sample-standard bracketing for mass bias correction. The Zn isotope compositions of the top surface of Fe-Mn crusts are in the range of 0.71‰ to 1.08‰, with a mean δ^{66}Zn value of 0.94‰±0.21‰ (2SD, n=28). The δ^{65}Cu values of the top surface of Fe-Mn crusts range from 0.33‰ to 0.73‰, with a mean value of 0.58‰±0.20‰ (2SD, n=28). The Cu isotope compositions of Fe-Mn crusts are isotopically lighter than that of dissolved Cu in deep seawater (0.58‰ vs. 0.9‰). In contrast, the δ^{66}Zn values of Fe-Mn crusts appear to be isotopically heavy compared to deep seawater (0.94‰±0.21‰ vs. 0.51‰±0.14‰). The isotope fractionation between Fe-Mn crusts and seawater is attributed to equilibrium partitioning between the sorption to crusts and the organic-ligand-bound Cu and Zn in seawater. The Cu and Zn isotopes in the top surface of Fe-Mn crusts are not a direct reflection of the Cu and Zn isotopes, but a function of Cu and Zn isotopes in modern seawater. This study proposes that Fe-Mn crusts have the potential to be archives for paleoceanography through Cu and Zn isotope analysis.

Key words: ferromanganese crusts, Cu isotopes, Zn isotopes, paleoceanography

Citation: He Lianhua, Liu Jihua, Zhang Hui, Gao Jingjing, Zhu Aimei, Zhang Ying. 2021. Copper and zinc isotope variations in ferromanganese crusts and their isotopic fractionation mechanism. Acta Oceanologica Sinica, 40(9): 43–52, doi: 10.1007/s13131-021-1775-5

1 Introduction

In recent years, with the development of stable isotope analysis techniques, transition metal isotopes have been increasingly developed in the marine science and earth science. First, as most transition metals are essential for primary productivity and are involved in diagenesis and mineralization (Bruland and Lohan, 2003; Morel and Price, 2003), the attendant isotopic fractionations are especially important for understanding diagenesis and mineralization and the detailed processes controlling their biological cycling on the modern and ancient earth (Beard et al., 1999; Pichat et al., 2003; John et al., 2007; Navarrete et al., 2011). Second, since the speciation and oxidation of transition metals in the ocean are redox sensitive, their isotope systems may have some potential applications in tracking the past redox states of the ocean (Albarède and Beard, 2004; Vance et al., 2008; Mason et al., 2005; Anbar and Rouxel, 2007; Fujii et al., 2011; Little et al., 2014b, 2017). For the latter potential application, previous researchers have made great progress with Mo isotopes (Anbar and Rouxel, 2007; Scott and Lyons, 2012). However, the Mo isotope system is usually used in euxinic settings (McManus et al., 2006; Poulson et al., 2006; Poulson Brucker et al., 2009; Siebert et al., 2006; Nägler et al., 2011; Scott and Lyons, 2012). There is a clear need to harness more potentially complementary information that may be held in broadly applicable transition metal isotopic systems. Cu and Zn are both widely distributed in various minerals, rocks, fluids and organisms in nature and involved in diagenesis, mineralization, hydrothermal activity and biological processes (Boyle et al., 1977; Bruland, 1980). The Cu and Zn isotope systems may provide new clues and evidence for revealing various geological and biological processes in the ocean.

Fe-Mn crusts have proven potential as archives of past chemical and isotopic compositions of various elements dissolved in oceanic deep water. This record is due to their formation through slow accumulation of seawater-derived Fe- and Mn-oxyhydroxide colloids on hard substrates such as volcanic seamounts that are kept free of sediment for millions of years (Craig et al., 1982; Halbach et al., 1983; Hein et al., 1988, 1992; Koschinsky and Halbach, 1995). Fe-Mn crusts incorporate transition metals such as Mo, Cu and Zn during growth, resulting in 10^6 fold enrichments from seawater concentrations in authigenic sediments (Arrhenius and Bonatti, 1963; Bertine and Turekian, 1973; Piper and Williamson, 1977; Aplin and Cronan, 1985; Hein et al., 1997; Koschinsky and Hein, 2003; Marcus et al., 2004; Peacock and Sherman, 2007; Kashiwabara et al., 2009). Therefore, the Cu and Zn isotope fractionations of Fe-Mn crusts have important influence on the Cu and Zn isotope compositions of the ocean. Significant inform-

Foundation item: The Shandong Provincial Natural Science Foundation of China under contract No. ZR2014DP009; the China Ocean Mineral Resource Research and Development Association Research Program under contract Nos DY135-N-1-03, DY135-C1-1-04 and DY135-R2-1-03; the Fund of the Construction and Operation of Test and Technical Support System for Natural Resources Investigation and Evaluation.
*Corresponding author, E-mail: jihliu@fio.org.cn

ation about geological and biogeochemical processes may be gleaned from them. However, very few studies to date have addressed the potential of the Cu and Zn isotope systems as tracers for these processes. In the earliest study, Maréchal et al. (2000) reported that the δ^{66}Zn values of 40 Fe-Mn nodules range from 0.53‰ to 1.16‰, with a mean value of 0.90‰±0.28‰. The range of variation corresponds to 16 times to the analytical precision (±0.04‰ in the study). The δ^{66}Zn values of Fe-Mn nodules seem to regularly distribute amongst the different oceanic areas, and the authors inferred that the isotopic signal of Zn may trace the strength of seasonal variations of biological productivity. However, great distinction exists between nodules and crusts, although they have similar textures, mineral compositions, major metal elements and others. In a recent study, Little et al. (2014b) presented isotopic data for Cu and Zn in three Fe-Mn crusts, which yielded δ^{65}Cu=(0.44±0.23)‰ and δ^{66}Zn=(1.04±0.21)‰. The authors compared the Cu and Zn isotopes in Fe-Mn crusts and other sedimentary outputs to the Cu and Zn isotopes in the dissolved oceanic pool in order to understand the oceanic mass balance of Cu and Zn isotopes.

This study reports the Cu and Zn isotope compositions of the top surface of 28 Fe-Mn crusts and 2 Fe-Mn nodules. This approach allows us to (1) establish the Cu and Zn isotope variability presented in Fe-Mn crusts and (2) understand the Cu and Zn isotope fractionation mechanism in Fe-Mn crusts. Combining these data with major and trace element geochemistry, this study tries to understand the mechanism of Cu and Zn fractionation in Fe-Mn crusts and determine whether these crusts can be used as archives for seawater Cu and Zn isotope compositions.

2 Materials and methods

2.1 *Sampling and sample preparation*

The top surface layers of 28 Fe-Mn crust samples and 2 Fe-Mn nodules (1–3 mm in thickness) were analysed. Some samples were obtained from various collections in the Pacific Ocean. Most of them were collected by dredging during the China Ocean Mineral Resources R&D Association cruises. The geographic location of the samples is shown in Fig. 1. In the laboratory, the outermost layer of each crust was cut and ground into powders using an agate mortar.

2.2 *Reagents and standards*

All acids (GR grade) used in this study were further purified by sub-boiling distillation systems (DST-1000, Savillex, USA). Acids and standards were prepared using >18.2 MΩ H_2O from a Milli-Q water system (Millipore Corporation, USA). Sample digestion and ion exchange chromatographic separation of Cu and Zn were conducted in an ultra-clean laboratory using a Savillex® PFA beaker. Total procedural blanks were less than 10 ng for Zn and less than 15 ng for Cu.

Zn isotope ratios were measured relative to the standard reference material IRMM-3702, which has an offset of 0.30‰± 0.05‰ with respect to the Johnson Matthey (JMC) Lyon standard (Archer et al., 2017; Moeller et al., 2012). Cu isotope ratios were measured relative to the standard reference material IRMM-633, which has an offset of 0.01‰±0.05‰ with respect to the NIST SRM 976 Cu (Moeller et al., 2012). The δ^{66}Zn (‰) and δ^{65}Cu (‰) values in this paper are reported with respect to JMC-Lyon Zn and the NIST SRM 976 Cu standards using the following equations:

$$\delta^{66}\mathrm{Zn}_{\mathrm{JMC\_Lyon}} = \left(\frac{{}^{66}\mathrm{Zn}/{}^{64}\mathrm{Zn}_{\mathrm{sample}}}{{}^{66}\mathrm{Zn}/{}^{64}\mathrm{Zn}_{\mathrm{IRMM\_3702}}} - 1\right) \times 1\,000 + \delta^{66}\mathrm{Zn}_{\mathrm{IRMM\_3702-JMC\_Lyon}}. \quad (1)$$

$$\delta^{65}\mathrm{Cu}_{\mathrm{NIST976}} = \left(\frac{{}^{65}\mathrm{Cu}/{}^{63}\mathrm{Cu}_{\mathrm{sample}}}{{}^{65}\mathrm{Cu}/{}^{63}\mathrm{Cu}_{\mathrm{IRMM\_633}}} - 1\right) \times 1\,000 + \delta^{65}\mathrm{Cu}_{\mathrm{IRMM\_633-NIST976}}. \quad (2)$$

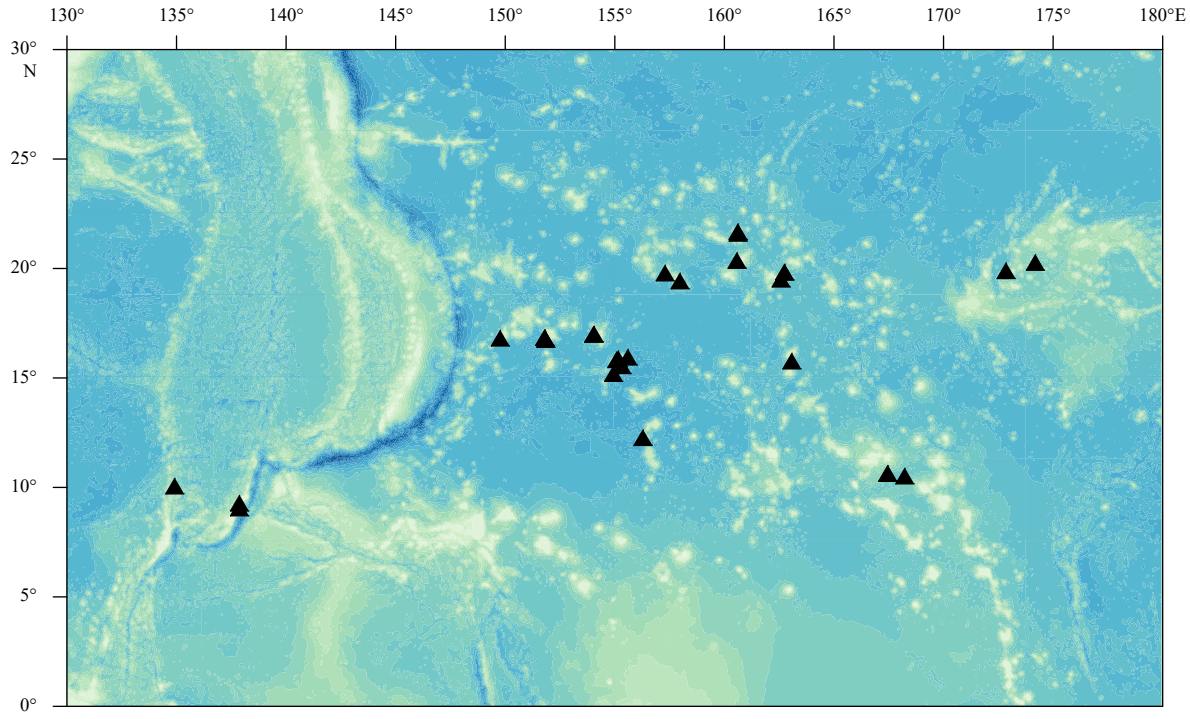

Fig. 1. Sample localities.

All sample preparation, isotopic measurements and element concentration measurements were performed at the Key Laboratory of Marine Geology and Metallogeny, First Institute of Oceanography, Ministry of Natural Resources, China.

2.3 *Element analysis*

Approximately (50±0.5) mg of powdered samples was weighed in Teflon pressure vials and digested in a mixture of 1 mL concentrated HNO_3 and 0.3 mL concentrated HCl in the oven at 190°C for 48 h. After evaporation at 150°C on hot plates, the solid residue was dissolved with 1 mL concentrated HNO_3 and then evaporated to dryness at 150°C. The solid residue was dissolved in 1 mL concentrated HNO_3. Meanwhile, 0.5 mL of 1.0 μg/g Rh solution was added as an internal standard. Then, the Teflon pressure vials were kept in the oven at 150°C for 12 h.

Major and trace element concentrations were measured by inductively coupled plasma optical emission spectrometry (ICP-OES) (iCAP6300, Thermofisher Scientific, USA) and quadrupole inductively coupled plasma mass spectrometry (ICP-MS) (X-Series 2, Thermofisher Scientific, USA). Precision was generally better than 6%. Geological reference materials of manganese crusts GBW07337 and GBW07338 were systematically analysed along with the samples, and the measured concentrations were within 5% uncertainty of the published concentration values (Gao et al., 2017).

2.4 *Isotopic analysis*

Approximately 30 mg of each sample was dissolved in 2 mL aqua regia and evaporated to dryness and then dissolved in 1 mL HF+HNO_3 mixture in order to eliminate silica. After evaporation, the residue was taken up in 0.2 mL concentrated HCl, and insoluble particles were centrifuged out. The supernatant was transferred into a clean beaker. The pellet was dissolved in HCl, evaporated to dryness at 110°C, and dissolved in 0.1 mL concentrated HCl, and the centrifugation procedure was repeated. Finally, all the supernatant was evaporated to dryness and dissolved in 1 mL 8.2 mol/L HCl.

The Cu and Zn fractions of all samples were separated from matrix components by ion exchange chemistry using a strongly basic anion resin (Bio-Rad macro-porous AG MP-1 M resin, 200–400 mesh). The PE columns (Bio-Rad, total volume of 10 mL) were filled with a total volume of 2 mL anion exchange resin, washed alternately with Milli-Q water and 0.5 mol/L HNO_3, and then preconditioned with 4 mL 8.2 mol/L HCl. Cu and Zn were eluted from the resin following a chromatographic procedure that was modified from Maréchal et al. (1999) (Table 1) (He et al., 2016). The purified Cu and Zn were evaporated to dryness, and 0.2 mL concentrated HNO_3 was added to remove residual organics that may have leached from the column. Cu and Zn recovery was measured by ICP-MS, and the recovery of all samples was 100%±5%.

Samples were re-dissolved in 2% HNO_3 at Cu or Zn concentrations of 200 ng/g. For Cu isotope measurements, samples were doped with 200 ng/g IRMM 3702 Zn as an internal calibrator element to correct instrument mass bias. Similarly, samples were doped with IRMM 633 Cu for Zn isotope measurements. The Cu and Zn isotope compositions were measured on a Nu Plasma multi-collector inductively coupled plasma mass spectrometer (MC-ICP-MS) in low-resolution mode. Samples were introduced via a desolvation nebulizer system (Nu DSN-100) at an uptake rate of 0.2 mL/min. Signal intensity was measured on masses 62, 63, 64, 65, 66, 67 and 68. Ni sampling cones were used, and ^{64}Ni was subtracted from ^{64}Zn by monitoring the signal from ^{62}Ni.

Table 1. Chromatographic separation procedure

Chromatographic column	AG MP-1 M resin
Clean resin	5 mL H_2O
Condition resin	4 mL 8.2 mol/L HCl
Load sample	1 mL 8.2 mol/L HCl
Remove matrix	7 mL 8.2 mol/L HCl + 0.001% H_2O_2
Elute Cu	20 mL 8.2 mol/L HCl + 0.01% HF + 0.001% H_2O_2
Elute Fe	15 mL 2 mol/L HCl + 0.001% H_2O_2
Remove matrix	2 mL 0.5 mol/L HNO_3
Elute Zn	7 mL 0.5 mol/L HNO_3

Samples were bracketed with a mixed standard of IRMM 3702 Zn and IRMM 633 Cu (mixture ratio around 1). Each measurement was preceded by an analysis of a 2% HNO_3 blank. These "on-peak zeroes" were used to correct sample signals for acid blanks. Data collection consisted of 2 blocks of 24 cycles with 4 s integration time.

Instrumental mass bias correction for Zn was achieved using a combination of sample-standard bracketing and Cu internal spike with spike-sample ratios around 1. If f_{Cu}=f_{Zn} (f represents mass bias factor), the slope of $\ln(^{65}Cu/^{63}Cu)_{meas}$ vs. $\ln(^{66}Zn/^{64}Zn)_{meas}$ should be 1.015 (Maréchal et al., 1999; Mason et al., 2004). The slope of $\ln(^{65}Cu/^{63}Cu)_{meas}$ vs. $\ln(^{66}Zn/^{64}Zn)_{meas}$ for a mixture of IRMM 3702 Zn standard and IRMM 633 Cu standard remains constant within a period of several hours. It may vary slightly from day to day, but it remains remarkably constant in a measurement session of several hours (Fig. 2). Long-term measurements show that the slope ranges from 0.93 to 1.10, normally less than 10%. Therefore, we consider that the mixture standards form a linear relationship with a slope the same as f_{Cu}= f_{Zn}. Zn data were corrected using Cu. Similarly, the mass bias for Cu was corrected using Zn.

The long term reproducibilities of the results were 0.08‰ for Cu and 0.04‰ for Zn. Cu isotope reproducibility was assessed by repeated measurements of the international standard IRMM 647 Cu, with $\delta^{65}Cu/^{63}Cu$ = 0.11‰±0.08‰ (n = 75). The reproducibility for Zn was assessed based on repeated analyses of an in-house standard MR-Zn. Zn reproducibility was very good for MR-Zn, and $\delta^{66}Zn/^{64}Zn$ = –9.48‰±0.04‰ (n = 57).

3 Results

3.1 *Element geochemistry*

Element contents and selected element ratios are presented in Table 2. Zn content is in the range of 484.3–1 039 μg/g, and Cu content varies between 0.02% and 0.79%. The Cu content in the Fe-Mn crusts varies little, and the Cu content in several Fe-Mn nodules is extremely high. The contents of other transition metals such as Co are around 800 μg/g, and the Ni content is homogenous in the range of 0.32%–1.06%. The average Mn content is around 24.35%, whereas the Fe content is around 15.92%. Phosphorus content varies between 0.21% and 0.78%, and Ca content is in the range of 1.67%–4.57%. It can be seen that P and Ca contents display a perfect correlation. This correlation is likely related to the fact that these two elements are essentially hosted in the authigenic phosphatic phase. Lithogenic element contents are in the range of 0.30% to 2.18% for Al, and Ti content yields an average value of 1.02%.

Zn/Mn ratios for Fe-Mn crusts and Fe-Mn nodules are similar. The mean Zn/Mn ratio for all the samples is 0.002 8. The

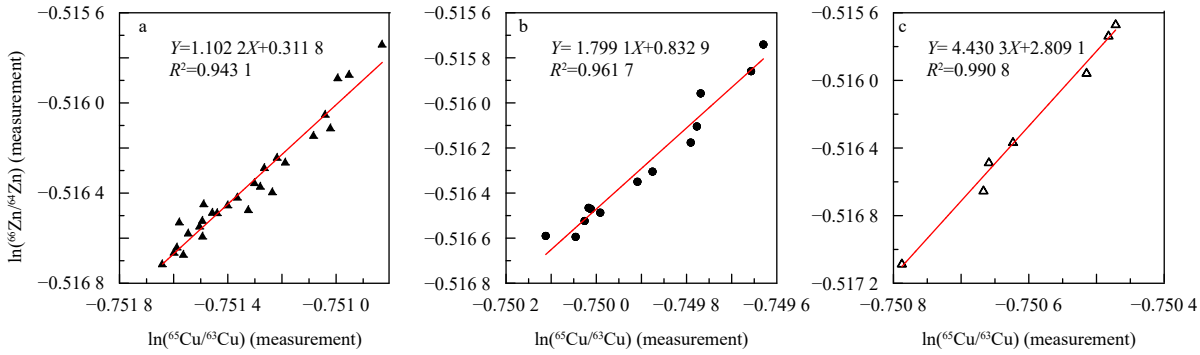

Fig. 2. Regression lines fitted through a mixed standard of IRMM 3702 Zn and IRMM 633 Cu during one single measurement session. a. 24 h analysis; b. 8 h analysis; c. 4 h analysis.

Table 2. Element contents and element content ratios of samples

Sample name	Al/%	Ca/%	Ti/%	P/%	Fe/%	Mn/%	Co/%	Cu/%	Zn/μg·g^{-1}	Co/Mn	Fe/Mn	Cu/Mn	Zn/Mn	Ni/Co	Ti/Al	Al/Fe	P/Ni
D001-8	0.65	2.84	0.98	0.34	14.35	27.45	0.42	0.18	725.30	0.015	0.52	0.006 7	0.002 6	1.69	1.51	0.045	0.48
D002-4	0.56	2.86	1.05	0.36	12.94	27.62	0.58	0.12	788.20	0.021	0.47	0.004 4	0.002 9	1.45	1.87	0.044	0.43
D91-1	0.69	3.38	0.82	0.56	17.07	23.47	0.72	0.03	564.30	0.030	0.73	0.001 3	0.002 4	0.62	1.18	0.041	1.28
D91A-1	1.01	3.10	0.82	0.53	17.94	21.39	0.61	0.03	530.80	0.029	0.84	0.001 6	0.002 5	0.61	0.81	0.056	1.40
D87-2	0.60	2.61	1.10	0.49	17.05	21.85	0.91	0.02	532.70	0.042	0.78	0.001 1	0.002 4	0.43	1.83	0.035	1.28
D31-2	0.63	2.66	1.43	0.42	17.14	26.52	1.10	0.06	726.20	0.042	0.65	0.002 2	0.002 7	0.56	2.27	0.037	0.67
D18-1	0.30	2.94	0.99	0.49	17.87	23.87	0.83	0.04	659.20	0.035	0.75	0.001 5	0.002 8	0.56	3.28	0.017	1.07
D71	0.62	3.32	1.05	0.56	15.88	25.98	1.07	0.05	623.00	0.041	0.61	0.001 8	0.002 4	0.50	1.69	0.039	1.06
D60-1	0.47	2.88	1.14	0.48	14.65	24.65	1.23	0.03	681.00	0.050	0.59	0.001 2	0.002 8	0.40	2.44	0.032	0.99
D008-1	1.32	2.37	1.22	0.41	16.78	22.43	0.77	0.13	698.00	0.034	0.75	0.005 9	0.003 1	0.70	0.92	0.078	0.75
D02-1-2	0.45	2.28	1.10	0.36	14.22	23.31	1.03	0.04	526.30	0.044	0.61	0.001 6	0.002 3	0.42	2.42	0.032	0.84
TG05-1	0.88	2.69	0.90	0.43	15.99	22.62	0.63	0.07	561.40	0.028	0.71	0.003 2	0.002 5	0.67	1.03	0.055	1.03
D55-1	1.86	2.63	1.06	0.38	16.66	20.89	0.53	0.20	732.20	0.026	0.80	0.009 5	0.003 5	0.86	0.57	0.112	0.83
JC-D70D	0.69	3.20	0.86	0.46	15.17	22.88	0.76	0.03	543.70	0.033	0.66	0.001 1	0.002 4	0.59	1.24	0.046	1.03
JC-D69A	0.74	2.35	1.27	0.35	17.20	25.74	1.12	0.06	530.00	0.044	0.67	0.002 5	0.002 1	0.36	1.71	0.043	0.87
D11-A-A-2	0.34	2.57	0.96	0.38	15.87	24.79	0.94	0.05	568.90	0.038	0.64	0.001 9	0.002 3	0.50	2.85	0.021	0.80
D19-1	0.30	2.53	0.86	0.36	12.93	26.40	1.13	0.05	698.60	0.043	0.49	0.001 9	0.002 6	0.60	2.82	0.024	0.52
D45	0.99	2.16	0.89	0.40	13.62	18.83	0.61	0.08	484.30	0.032	0.72	0.004 4	0.002 6	0.57	0.90	0.073	1.14
D48-1	1.09	2.46	0.85	0.48	17.43	23.27	0.62	0.20	941.60	0.027	0.75	0.008 7	0.004 0	0.93	0.78	0.063	0.84
D20-1	0.81	2.23	0.65	0.41	12.30	25.06	0.83	0.08	891.80	0.033	0.49	0.003 2	0.003 6	0.95	0.79	0.066	0.52
D16-1	1.27	4.57	2.13	0.78	31.41	37.92	1.75	0.06	1 039.00	0.046	0.83	0.001 7	0.002 7	0.41	1.68	0.041	1.08
D09-1	1.65	1.67	0.95	0.27	13.11	21.85	0.41	0.43	786.80	0.019	0.60	0.019 9	0.003 6	1.73	0.58	0.126	0.38
D66-2	1.56	1.68	0.83	0.26	11.49	23.22	0.37	0.51	902.50	0.016	0.49	0.021 9	0.003 9	2.16	0.53	0.136	0.32
FG2a	2.10	1.73	0.66	0.21	9.22	25.34	0.25	0.79	1 037.00	0.010	0.36	0.031 0	0.004 1	4.19	0.31	0.228	0.20
FG1	0.35	2.67	1.00	0.39	16.69	25.66	0.98	0.05	588.30	0.038	0.65	0.002 0	0.002 3	0.50	2.88	0.021	0.80
D105-13	1.71	1.78	1.00	0.30	14.15	22.83	0.44	0.35	767.40	0.019	0.62	0.015 4	0.003 4	1.63	0.59	0.121	0.42
D43-1*	2.18	2.00	1.39	0.28	16.73	20.20	0.49	0.26	573.10	0.024	0.83	0.012 7	0.002 8	0.87	0.64	0.130	0.67
D27-1a*	0.52	2.59	0.81	0.41	15.54	24.33	0.57	0.08	642.50	0.023	0.64	0.003 1	0.002 5	0.56	1.02	0.045	1.46
D61-2	0.51	2.71	1.23	0.48	16.21	25.36	1.35	0.03	606.80	0.053	0.64	0.001 1	0.002 4	0.34	2.39	0.032	1.04
D002-4-2	0.94	2.37	1.08	0.44	19.34	21.58	0.78	0.05	537.00	0.036	0.90	0.002 3	0.002 5	0.41	1.15	0.049	1.38

mean Cu/Mn ratio for Fe-Mn crusts is 0.004 1. The Cu/Mn ratios for Fe-Mn nodules vary between 0.004 and 0.031, which are slightly higher than those for Fe-Mn crusts. As observed in other studies, Zn/Mn and Cu/Mn ratios for Fe-Mn crusts exhibit more scatter. This feature is likely due to the non-conservative distribution of these two elements in ocean waters. As a widely used geochemical source tracer, the Fe/Mn ratio varies between 0.36 and 0.90, which is consistent with the values already reported for other Fe-Mn crusts in the ocean. Al/Fe ratios, which are used as an estimate of the lithogenic contribution, are in the range of 0.014 to 0.228. The other element ratio details can be seen in Table 2.

3.2 *Cu and Zn isotope ratios*

Cu and Zn isotope data, together with sample locations and water depth, are listed in Table 3. Overall, the δ^{66}Zn values are in the range of 0.71‰ to 1.08‰, with a mean value of 0.94‰± 0.21‰ at the 95% confidence level. Cu isotope compositions seem slightly more variable. Sample D27-1a* shows a very heavy Cu isotope composition with δ^{65}Cu=0.91‰. Overall, the δ^{65}Cu values range between 0.33‰ and 0.91‰, with a mean value of 0.58‰±0.20‰ at the 95% confidence level. Although the observed variations for Cu and Zn isotope compositions exceed the reproducibility of the measurements (i.e., 0.08‰ for Cu and

Table 3. Cu and Zn isotope ratios of samples

Sample name	Depth/m	Latitude	Longitude	$\delta^{66}Zn_{IRMM3702}$/‰	$\delta^{66}Zn_{JMC\text{-}Lyon}$/‰	$\delta^{65}Cu_{IRMM633}$/‰	$\delta^{65}Cu_{NIST976}$/‰
D001-8	2 169	19°30.84′N	162°35.83′E	0.63	0.93	0.47	0.48
D002-4	2 198	19°50.09′N	162°45.47′E	0.71	1.01	0.64	0.65
D91-1	1 634	16°50.67′N	151°49.02′E	0.51	0.81	0.56	0.57
D91A-1	1 865	16°50.39′N	151°48.70′E	0.62	0.92	0.55	0.56
D87-2	1 539	16°45.52′N	151°51.55′E	0.78	1.08	0.56	0.57
D31-2	2 363	19°47.71′N	157°18.40′E	0.67	0.97	0.61	0.62
D18-1	2 596	19°25.93′N	157°59.11′E	0.57	0.87	0.67	0.68
D71	1 958	20°16.67′N	174°12.11′E	0.49	0.79	0.32	0.33
D60-1	1 657	19°54.01′N	172°51.87′E	0.52	0.82	0.67	0.68
D008-1	2 514	17°00.34′N	154°04.25′E	0.41	0.71	0.36	0.37
D02-1-2	2 997	16°59.68′N	154°02.57′E	0.78	1.08	0.60	0.61
TG05-1	2 456	16°49.18′N	149°46.96′E	0.50	0.80	0.58	0.59
D55-1	1 481	10°03.82′N	134°55.73′E	0.56	0.86	0.53	0.54
JC-D70D	2 722	15°33.53′N	155°20.09′E	0.75	1.05	0.59	0.60
JC-D69A	4 578	15°57.04′N	155°36.76′E	0.68	0.98	0.63	0.64
D11A-A-1	2 600	10°31.34′N	168°14.53′E	0.64	0.94	0.71	0.72
D19-1	2 280	10°38.30′N	167°27.96′E	0.74	1.04	0.68	0.69
D45	1 400	21°41.15′N	160°37.87′E	0.53	0.83	0.48	0.49
D48-1	1 960	21°36.52′N	160°38.06′E	0.68	0.98	0.54	0.55
D20-1	2 747	20°22.09′N	160°35.17′E	0.72	1.02	0.72	0.73
D16-1	1 566	15°52.65′N	155°10.33′E	0.75	1.05	0.67	0.68
D09-1	2 836	15°12.26′N	154°57.27′E	0.51	0.81	0.57	0.58
FG2a	1 593	9°16.99′N	137°52.97′E	0.74	1.04	0.44	0.45
FG1	1 666	9°03.75′N	137°49.84′E	0.66	0.96	0.63	0.64
D105-13	2 280	10°38.30′N	167°28.02′E	0.70	1.00	0.57	0.58
D27-1a*	2 136	12°16.64′N	156°17.72′E	0.76	1.06	0.90	0.91
D66-2	1 912	15°46.42′N	163°05.32′E	0.61	0.91	0.43	0.44
D61-2	1 805	15°29.97′N	155°05.94′E	0.73	1.03	0.59	0.60
D002-4-2	2 198	19°50.09′N	162°45.47′E	0.72	1.02	0.67	0.68
D43-1*	4 661	18°09.80′N	179°41.75′W	0.59	0.89	0.43	0.44

0.04‰ for Zn), the ranges fall within the ranges of previously published data.

4 Discussion

4.1 *Isotopic variability of Cu and Zn in the top surface of Fe-Mn crusts*

One of the striking results from this study is that the Cu and Zn isotope compositions of the top surface of Fe-Mn crusts and Fe-Mn nodules. The $\delta^{66}Zn$ values of the two Fe-Mn nodules (D27-1a* and D43-1*) are 1.06‰ and 0.89‰, which are consistent with previous studies. The Zn isotope compositions of the top surface of Fe-Mn crusts are in the range of 0.71‰ to 1.08‰, with a mean value of 0.94‰±0.21‰. There is no significant variation in the isotopic compositions of Zn in Fe-Mn crusts and Fe-Mn nodules. However, the deviation from Fe-Mn crusts is significant compared to the analytical uncertainty associated with the long-term reproducibility. The sample with the lowest $\delta^{66}Zn$ is D008-1, which is a platy crust, with pale yellow bedrock, loose and granular surface, and mixed with yellow impurities. The sample with the highest $\delta^{66}Zn$ (D02-1-2) is a pebble crust, with dark brown surface. The appearance of these two crust samples is quite different.

For Cu, the sample with abnormally high $\delta^{65}Cu$ (D27-1a*, $\delta^{65}Cu$=0.91‰) is a Fe-Mn nodule. This nodule is oval, about 2 cm in diameter, with nodular protrusions, and the surface of the nodules is bright black with traces of biological activity (Fig. 3). The abnormally high Cu isotope ratio may be linked to marine biological activity on the surface of the nodules. Another Fe-Mn nodule sample has a Cu isotope ratio of 0.44‰. The $\delta^{65}Cu$ values of all Fe-Mn crusts samples range from 0.33‰ to 0.73‰, with a mean value of 0.58‰±0.20‰. This shift is over two times greater than the analytical uncertainty on the measurements.

The precise reason why the Cu and Zn isotopic compositions of the top surface of Fe-Mn crusts vary is not clear. Because Fe-Mn crusts grow very slowly, typically at a rate of millimetres per thousand years, the significance of their geochemical properties is distorted by the long-time coverage even by the smallest samples. Maréchal et al. (2000) reported that higher values of $\delta^{66}Zn$ in ferromanganese nodules are preferentially associated with temperate and subpolar latitudes. They ascribed the isotopic fluctuations to the seasonal variation of primary productivity. However, in this study, the $\delta^{66}Zn$ and $\delta^{65}Cu$ values of the top surface of Fe-Mn crusts do not show visibly variability with latitudes. Chlorophyll concentration of phytoplankton in seawater is an important observational parameter in these investigation stations. It is not only an index characterizing phytoplankton biomass, but also can be used to estimate the primary productivity of a given sea area. In this study, most of higher $\delta^{66}Zn$ and $\delta^{65}Cu$ values are associated with higher chlorophyll concentration. However, in some stations, the chlorophyll concentration is relatively low but the $\delta^{65}Cu$ and $\delta^{66}Zn$ values are high. Considering that fractionation also occurs during the formation of Fe-Mn crusts, this study infers that the local productivity and remineralization may account for the Cu and Zn isotopic variations in Fe-Mn crusts. However, it is difficult to explain the distribution of $\delta^{66}Zn$ and $\delta^{65}Cu$ in Fe-Mn crusts with these limited data. More re-

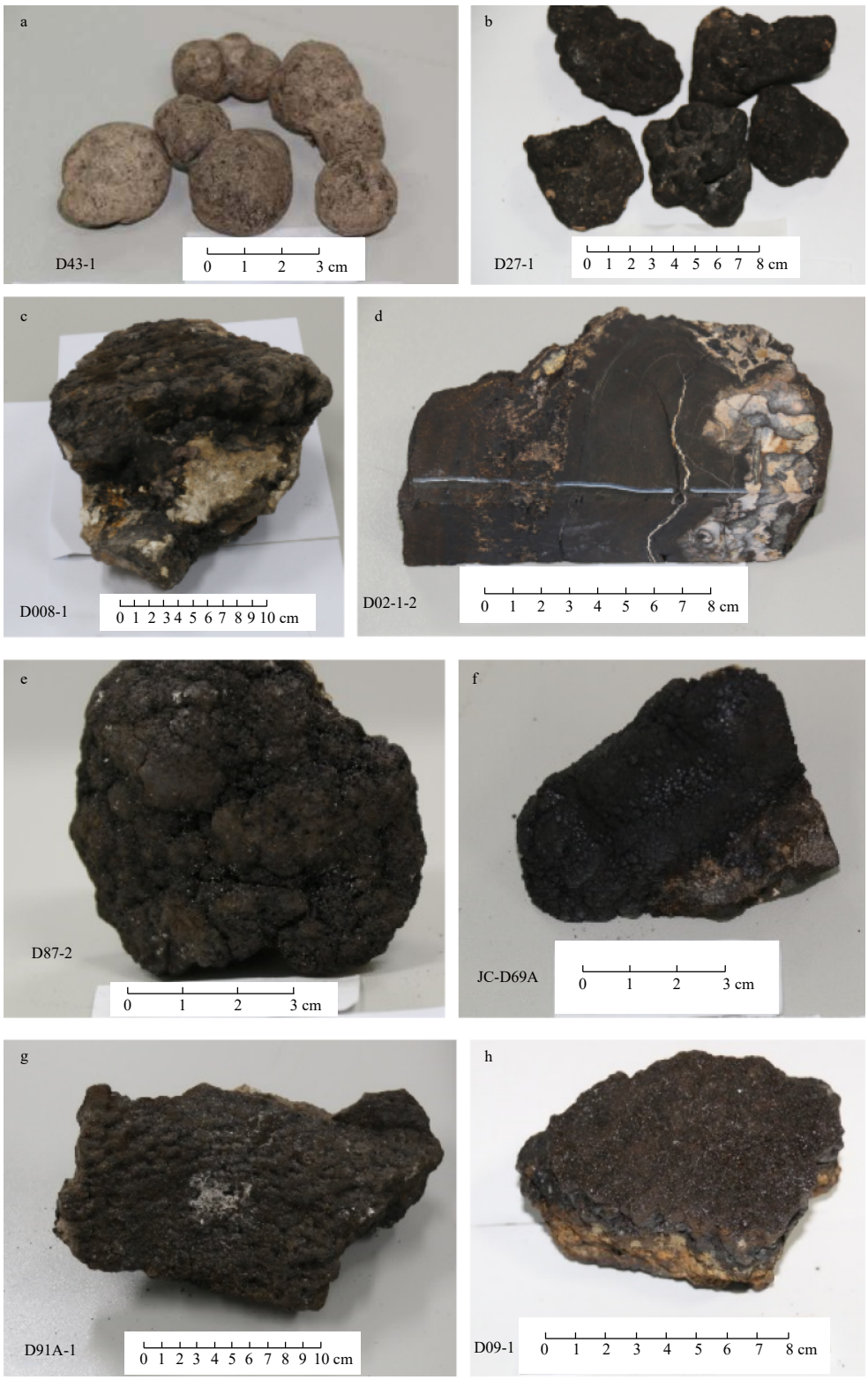

Fig. 3. Photographs of Fe-Mn nodule samples and Fe-Mn crust samples.

lated research is needed.

4.2 *Relationship with seawater Cu and Zn isotope composition*

Fe-Mn crusts and Fe-Mn nodules represent useful analogues for the dispersed Fe-Mn oxide phases presented throughout oxic marine sediments. They grow very slowly, typically at rates of millimetres per thousand years. Dissolved Cu and Zn in the seawater are adsorbed and incorporated into Fe-Mn crusts during their formation. Do the Cu and Zn isotope compositions of the top surface of Fe-Mn crusts reflect the average isotopic composition of ocean deep water? It is necessary to compare the isotopic compositions of the top surface of Fe-Mn crusts with those of

seawater. The first dataset of dissolved δ^{65}Cu in seawater from Pacific Ocean, India Ocean and English channel was published by Vance et al. (2008) and reported δ^{65}Cu ranging from 0.90‰ to 1.44‰. More recently, three Pacific Ocean δ^{65}Cu vertical profiles were measured, ranging from 0.61‰ to 0.78‰ (Boyle et al., 2012; Thompson et al., 2013; Thompson and Ellwood, 2014). Takano et al. (2014) also investigated several profiles in the Pacific and focused mostly on surface layers. However, these profiles show that most of the seawater δ^{65}Cu composition variability occurs in the photic zone but is relatively homogenised in the deeper waters. Overall, previous studies give the δ^{65}Cu of seawater at around 0.9‰±0.3‰. In general, the δ^{65}Cu value is higher than 0.9‰ when samples below 1 000 m. Compared to those for Cu, there are more published data for the Zn isotope composition of seawater. The repeated findings to date in studies of the Zn isotope composition of seawater, representing nearly 700 isotope analyses from Southern Ocean and NE Pacific values (Vance et al., 2012) and 6 depth profiles from the equatorial Atlantic (Boyle et al., 2012) demonstrate that the deep ocean (beneath 1 000 m) is extremely homogeneous. Excluding data that have been specifically identified by the authors as impacted by local hydrothermal and benthic sources, nearly 300 analyses of this dominant deep ocean give a δ^{66}Zn=0.51‰±0.14‰. A comparison of these results with the data of this study for Fe-Mn crusts provides interesting observations. First, the Cu isotope compositions of the Fe-Mn crusts range from 0.33‰ to 0.73‰, with a mean value of 0.58‰± 0.20‰. Even the highest δ^{65}Cu value (0.73‰) is distinctly isotopically lighter than the Cu isotopic composition in deep seawater at around 0.9‰. On the other hand, the δ^{66}Zn values of the Fe-Mn crusts (0.94‰±0.21‰) appear to be isotopically heavy compared to deep seawater (0.51‰±0.14‰). Overall, the isotopic separation between seawater and the top surface of Fe-Mn crusts ($\Delta_{\text{Fe-Mn crusts-seawater}}$) is -0.3‰ for Cu and 0.4‰ for Zn. This also implies that the Cu and Zn isotopes in the outmost layer of Fe-Mn crusts are not a direct reflection of the Cu and Zn isotopes in modern seawater, but only a function of the Cu and Zn isotopes in modern seawater.

The source effects on the $\Delta_{\text{Fe-Mn crusts-seawater}}$ are almost certainly negligible, as all samples derived from the continental crust and the mantle fall with a relatively narrow range of δ^{66}Zn at approximately 0.3‰ and δ^{65}Cu at 0.00‰. According to the element geochemistry, Co/Mn, Cu/Mn, Fe/Mn, and Zn/Mn are similar between the crusts, which suggest that growth rates or seawater mass parameters are not the major controls on the enrichments in Cu and Zn in these crusts. Some of the variations in Zn/Al, Cu/Al and Zn and Cu enrichment factors in the Fe-Mn crusts may be due to differences in the accumulation rates of Cu and Zn, perhaps associated with differing deep ocean Cu and Zn concentrations. However, Cu and Zn isotope ratios do not show any variations with depth (Fig. 4), thus once again proved that Cu and Zn isotopes are homogenous in deep water.

4.3 *Mechanisms of isotopic fractionation*

Possible explanations for the difference between Cu and Zn isotope compositions for Fe-Mn crusts and seawater are (1) biologically mediated fractionation of Cu and Zn in seawater; (2) adsorption and incorporation of Cu and Zn in seawater during formation of Fe-Mn crusts accompanied by isotopic fractionation; (3) fractionation associated with differences in Cu and Zn speciation in seawater or (4) a combination of these factors. However, the precise fractionation mechanisms are not clear.

Cu and Zn are both strongly cycled between the surface water and the deep ocean. Zn concentrations are approximately 2 nmol/L and 10 nmol/L in the deep Pacific (e.g., Bruland, 1980; Bruland et al., 1994; Lohan et al., 2002; Boyle et al., 2012). However, in the photic zone, Zn concentrations are often less than 0.1 nmol/L. The strong depletion in the surface ocean is due to biological uptake (Morel and Price, 2003), and regeneration from the deep ocean drives up the concentrations. Similarly, the Cu concentration profile shows depletion in the surface water and enrichment in the deep ocean. Both Cu and Zn are bioessential elements and dominated by complexation with strong organic ligands in the surface ocean (Coale and Bruland, 1988; Bruland, 1989; Donat and Bruland, 1990; Moffett and Dupont, 2007). Biological processes are usually accompanied by kinetic fractionation, where the lighter isotope is preferentially concentrated in the biomass, forcing the residual reservoir to form a heavier isotopic composition (Valley and Cole, 2001). Fe-Mn crusts are formed through the slow precipitation of Fe-Mn colloids in seawater. Metal cations in seawater, such as Cu and Zn, are incorporated with Fe-Mn colloids and can further precipitate through slow uptake onto the Fe-Mn crust surface. In this study, Zn con-

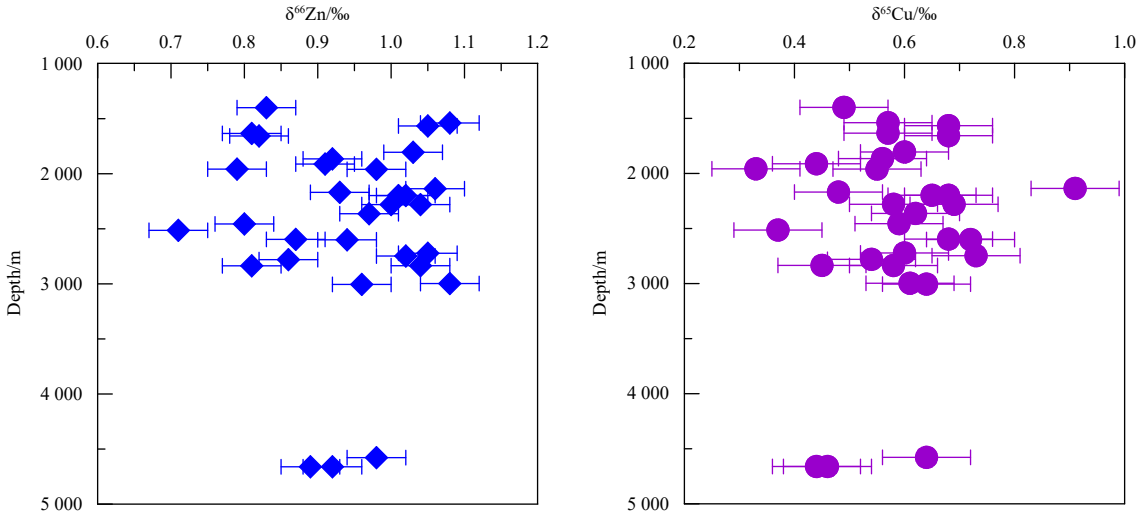

Fig. 4. Cu and Zn isotope ratios of Fe-Mn crusts collected at different depths. The error bars correspond to ±0.04‰ for Zn and ±0.08‰ for Cu.

tent in the Fe-Mn crusts is in the range of around 484 μg/g to 1 039 μg/g, and Cu content varies from 200 μg/g to 7 900 μg/g. A plot of the Cu and Zn isotope compositions of Fe-Mn crusts against their contents is shown in Fig. 5. The Cu and Zn isotope ratios do not visibly vary with Cu and Zn contents, which may imply that isotopic fractionation due to biological activity in the surface ocean is not responsible for Cu and Zn isotope ratios in Fe-Mn crusts. Previous studies also indicate that Cu and Zn are isotopically homogeneous in deep seawater, so it is impossible to cause large variations in Cu and Zn isotope ratios in Fe-Mn crusts. The Cu and Zn isotope compositions of the Fe-Mn crusts are unrelated to their Co contents (Fig. 5). Therefore, the Cu and Zn isotope compositions are independent of the growth rate (Halbach et al., 1983).

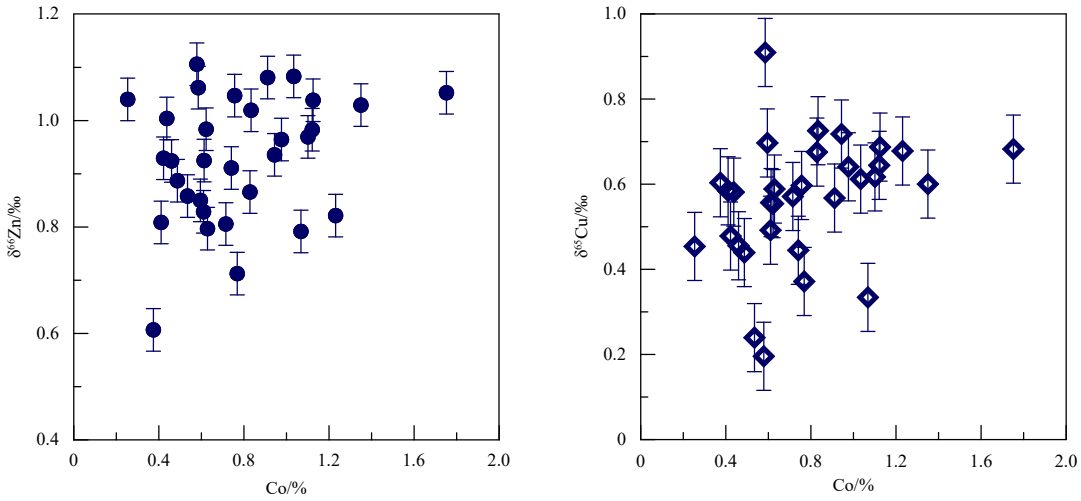

Fig. 5. Cu and Zn isotope ratios of Fe-Mn crusts plotted against their Co contents. The error bars correspond to ±0.04‰ for Zn and ±0.08‰ for Cu.

The Cu and Zn isotope variations may be associated with equilibrium partitioning between the sorption to crusts and the organic-ligand-bound Cu and Zn in seawater. Stable isotope fractionations are ordered by the rule that heavy isotopes tend to accumulate in substances with stronger bonds. This process means that heavy isotopes tend to bind with smaller coordination numbers (Schauble, 2004). Fe-Mn crusts are formed through slow precipitation of Fe-Mn colloids in seawater. The surface of the crust is exposed to seawater for a long time. It is possible that adsorbed Cu and Zn on the Fe-Mn crust surface are continuously incorporated into the mineral structure. This process would allow isotopic exchange of Cu and Zn with seawater. It has been shown that free Cu^{2+} in seawater is dominated by V-fold coordination, forming a hydrate $[Cu(H_2O)_5]^{2+}$ complex (Pasquarello et al., 2001; Amira et al., 2005). Cu on Fe-Mn crusts is mainly in Ⅲ- to Ⅳ-fold coordination (around 65%), with limited Ⅵ-fold structural incorporation (around 35%) (Little et al., 2014a). The balance of surface complexation and structural incorporation indicates that Fe-Mn crusts favour sorption of heavy Cu isotopes. Free Zn^{2+} in seawater is Ⅵ-fold coordinated in the $[Zn(H_2O)_6]^{2+}$ complex and Ⅳ-fold coordinated in Fe-Mn crusts. Thus, Fe-Mn crusts also favour sorption of heavy Zn isotopes. If all the Cu and Zn elements in the Fe-Mn crust come from free Cu^{2+} and free Zn^{2+} in seawater, then the $\delta^{65}Cu$ and $\delta^{66}Zn$ values in the Fe-Mn crust should be higher than that in seawater. However, Cu and Zn are dominantly complexed to organic ligands in seawater. Free Cu^{2+} is less than 0.1% of the total dissolved fraction. Free Zn^{2+} is also very limited in seawater. Therefore, the isotopic fractionation of Cu and Zn in crusts is only a part of the total isotope separation between sorbed Cu and Zn and that dissolved in seawater relative to free Cu^{2+} and free Zn^{2+}. Partitioning between the free phase and the ligand-bound phase is equally important. The organic-ligand complexations favour heavy isotopes. Cu is strongly complexed to organic ligands in seawater, which can explain why Cu in seawater is isotopically heavier than Fe-Mn crusts. For Zn, the strong organic-ligand complexations appear to be restricted in the surface ocean. Half of dissolved inorganic Zn is complexed by chloride ions, and the chloride ions prefer to complex light Zn isotopes. Thus, heavy Zn in seawater is incorporated on the surface of Fe-Mn crusts, making the Zn isotope composition of Fe-Mn crusts heavier.

4.4 *Significance as paleoceanographic tracers*

What exactly controls the fractionation of Cu and Zn isotopes in Fe-Mn crusts is still under research. In summary, possible explanations are (1) changes in Cu and Zn isotopic composition in seawater, and (2) changes in marine environment during the formation of Fe-Mn crusts. The relatively long oceanic residence time of Cu and Zn in comparison to the around 1 500 a mixing time of oceans, making the distribution of Cu and Zn in deep waters is relatively well-mixed and homogenous. Regardless of the fractionation mechanism, the isotopic composition of Cu and Zn in Fe-Mn crusts is a function of Cu and Zn isotopes in seawater. The $\delta^{66}Zn$ and $\delta^{65}Cu$ values of each layer in Fe-Mn crust actually reflect the isotopic composition of Cu and Zn in seawater during their respective formation periods. Considering the relatively long residence times of Cu and Zn in the deep ocean, changes in either Cu and Zn input to or output from seawater have been recorded in crusts. One may presume that different Cu and Zn isotope records between different layers from the same Fe-Mn crusts reflect either local sources or changes in the Cu and Zn isotope fractionation factors. Assuming that the known functional relationship between the Cu and Zn isotopes in seawater and the Cu and Zn isotopes in the Fe-Mn crust, it would be more convenient to understand ancient ocean water by analysis the Cu and Zn isotope compositions in the Fe-Mn crusts. The potential

of Cu and Zn isotope compositions for palaeoceanography through Fe-Mn crust analysis becomes quite appealing.

5 Conclusions

In this study, the geochemical composition and Cu and Zn isotope compositions of the top surface layer of 28 Fe-Mn crusts and 2 Fe-Mn nodules were reported.

(1) The Zn isotope composition of the top surface of Fe-Mn crusts are in the range of 0.71‰ to 1.08‰, with a mean δ^{66}Zn value of 0.94‰±0.21‰ (2SD, n=28). The δ^{65}Cu values of Fe-Mn crusts range from 0.33‰ to 0.73‰, with a mean value of 0.58‰±0.20‰. The Cu and Zn isotope ratios of these two Fe-Mn nodules together with published data show no significant variation between Fe-Mn nodules and Fe-Mn crusts.

(2) The Cu isotope compositions of Fe-Mn crusts are isotopically lighter than that of dissolved Cu in deep seawater (0.58‰ vs. 0.9‰). On the other hand, the δ^{66}Zn values of the Fe-Mn crusts appear to be isotopically heavy compared to the deep seawater (0.94‰±0.21‰ vs. 0.51‰±0.14‰).

(3) The precise fractionation mechanisms for the fractionations between Fe-Mn crusts and seawater are not clear. It is thought to be due to equilibrium partitioning between the sorption to crusts and the organic-ligand-bound Cu and Zn in seawater. The Cu and Zn isotopes in the top surface of Fe-Mn crusts are not a direct reflection of the Cu and Zn isotopes, but a function of Cu and Zn isotopes in modern seawater. Fe-Mn crusts have the potential to be archives for paleoceanography through Cu and Zn isotope analysis.

References

Amira S, Spångberg D, Hermansson K. 2005. Distorted five-fold coordination of Cu^{2+}(*aq*) from a Car-Parrinello molecular dynamics simulation. Physical Chemistry Chemical Physics, 7(15): 2874–2880, doi: 10.1039/b502427g

Anbar A D, Rouxel O. 2007. Metal stable isotopes in paleoceanography. Annual Review of Earth and Planetary Sciences, 35(1): 717–746, doi: 10.1146/annurev.earth.34.031405.125029

Aplin A C, Cronan D S. 1985. Ferromanganese oxide deposits from the Central Pacific Ocean: I. Encrustations from the Line Islands Archipelago. Geochimica Et Cosmochimica Acta, 49(2): 427–436, doi: 10.1016/0016-7037(85)90034-1

Archer C, Andersen M B, Cloquet C, et al. 2017. Inter-calibration of a proposed new primary reference standard AA-ETH Zn for zinc isotopic analysis. Journal of Analytical Atomic Spectrometry, 32(2): 415–419, doi: 10.1039/C6JA00282J

Albarède B, Beard B. 2004. Analytical methods for non-traditional isotopes in geochemistry of non-traditional stable isotopes. Reviews in Mineralogy & Geochemistry, 55: 113–152

Arrhenius G, Bonatti E. 1963. Neptunism and vulcanism in the ocean. Progress in Oceanography, 3: 7–22

Beard B L, Johnson C M, Cox L, et al. 1999. Iron isotope biosignatures. Science, 285(5435): 1889–1892, doi: 10.1126/science.285.5435.1889

Bertine K K, Turekian K K. 1973. Molybdenum in marine deposits. Geochimica et Cosmochimica Acta, 37(6): 1415–1434, doi: 10.1016/0016-7037(73)90080-X

Boyle E A, Edmond J M, Sholkovitz E R. 1977. The mechanism of iron removal in estuaries. Geochimica et Cosmochimica Acta, 41(9): 1313–1324, doi: 10.1016/0016-7037(77)90075-8

Boyle E A, John S, Abouchami W, et al. 2012. GEOTRACES IC1(BATS) contamination-prone trace element isotopes Cd, Fe, Pb, Zn, Cu, and Mo intercalibration. Limnology and Oceanography: Methods, 10(9): 653–665, doi: 10.4319/lom.2012.10.653

Bruland K W. 1980. Oceanographic distributions of cadmium, zinc, nickel, and copper in the North Pacific. Earth and Planetary Science Letters, 47(2): 176–198, doi: 10.1016/0012-821X(80)90035-7

Bruland K W. 1989. Complexation of zinc by natural organic ligands in the Central North Pacific. Limnology and Oceanography, 34(2): 269–285, doi: 10.4319/lo.1989.34.2.0269

Bruland K W, Lohan M C. 2003. Controls of trace metals in seawater. Treatise on Geochemistry, 6: 23–47

Bruland K W, Orians K J, Cowen J P. 1994. Reactive trace metals in the stratified central North Pacific. Geochimica et Cosmochimica Acta, 58(15): 3171–3182, doi: 10.1016/0016-7037(94)90044-2

Coale K H, Bruland K W. 1988. Copper complexation in the Northeast Pacific. Limnology and Oceanography, 33(5): 1084–1101, doi: 10.4319/lo.1988.33.5.1084

Craig J D, Andrews J E, Meylan M A. 1982. Ferromanganese deposits in the Hawaiian Archipelago. Marine Geology, 45(1–2): 127–157, doi: 10.1016/0025-3227(82)90183-9

Donat J R, Bruland K W. 1990. A comparison of two voltammetric techniques for determining zinc speciation in Northeast Pacific Ocean waters. Marine Chemistry, 28(4): 301–323, doi: 10.1016/0304-4203(90)90050-M

Fujii T, Moynier F, Dauphas N, et al. 2011. Theoretical and experimental investigation of nickel isotopic fractionation in species relevant to modern and ancient oceans. Geochimica et Cosmochimica Acta, 75(2): 469–482, doi: 10.1016/j.gca.2010.11.003

Gao Jingjing, Liu Jihua, Li Xianguo, et al. 2017. The determination of 52 elements in marine geological samples by an inductively coupled plasma optical emission spectrometry and an inductively coupled plasma mass spectrometry with a high-pressure closed digestion method. Acta Oceanologica Sinica, 36(1): 109–117, doi: 10.1007/s13131-017-0991-5

Halbach P, Segl M, Puteanus D, et al. 1983. Co-fluxes and growth rates in ferromanganese deposits from central Pacific seamount areas. Nature, 304(5928): 716–719, doi: 10.1038/304716a0

He Lianhua, Liu Jihua, Zhang Jun, et al. 2016. Separation of Cu and Zn in cobalt-rich crusts for isotope determination by MC-ICP MS. Journal of Instrumental Analysis (in Chinese), 35(10): 1347–1350

Hein J R, Bohrson W A, Schulz M S, et al. 1992. Variations in the fine-scale composition of a central Pacific ferromanganese crust: Paleoceanographic implications. Paleoceanography, 7(1): 63–77, doi: 10.1029/91PA02936

Hein J R, Koschinsky A, Halbach P, et al. 1997. Iron and Manganese Oxide Mineralization in the Pacific. Geological Society, London, Special Publications, 119(1): 123–138, doi: 10.1144/GSL.SP.1997.119.01.09

Hein J R, Schwab W C, Davis A S. 1988. Cobalt- and platinum-rich ferromanganese crusts and associated substrate rocks from the Marshall Islands. Marine Geology, 78(3–4): 255–283, doi: 10.1016/0025-3227(88)90113-2

John S G, Geis R W, Saito M A, et al. 2007. Zinc isotope fractionation during high-affinity and low-affinity zinc transport by the marine diatom *Thalassiosira oceanica*. Limnology and Oceanography, 52(6): 2710–2714, doi: 10.4319/lo.2007.52.6.2710

Kashiwabara T, Takahashi Y, Tanimizu M. 2009. A XAFS study on the mechanism of isotopic fractionation of molybdenum during its adsorption on ferromanganese oxides. Geochemical Journal, 43(6): e31–e36, doi: 10.2343/geochemj.1.0060

Koschinsky A, Halbach P. 1995. Sequential leaching of marine ferromanganese precipitates: Genetic implications. Geochimica et Cosmochimica Acta, 59(24): 5113–5132, doi: 10.1016/0016-7037(95)00358-4

Koschinsky A, Hein J R. 2003. Uptake of elements from seawater by ferromanganese crusts: solid-phase associations and seawater speciation. Marine Geology, 198(3–4): 331–351, doi: 10.1016/S0025-3227(03)00122-1

Little S H, Sherman D M, Vance D, et al. 2014a. Molecular controls on Cu and Zn isotopic fractionation in Fe-Mn crusts. Earth and Planetary Science Letters, 396: 213–222, doi: 10.1016/j.epsl.2014.04.021

Little S H, Vance D, McManus J, et al. 2017. Copper isotope signatures in modern marine sediments. Geochimica et

Cosmochimica Acta, 212: 253–273, doi: 10.1016/j.gca.2017.06.019
Little S H, Vance D, Walker-Brown C, et al. 2014b. The oceanic mass balance of copper and zinc isotopes, investigated by analysis of their inputs, and outputs to ferromanganese oxide sediments. Geochimica et Cosmochimica Acta, 125: 673–693, doi: 10.1016/j.gca.2013.07.046
Lohan M C, Statham P J, Crawford D W. 2002. Total dissolved zinc in the upper water column of the subarctic North East Pacific. Deep-Sea Research Part II: Topical Studies in Oceanography, 49(24–25): 5793–5808, doi: 10.1016/S0967-0645(02)00215-1
Marcus M A, Manceau A, Kersten M. 2004. Mn, Fe, Zn and As speciation in a fast-growing ferromanganese marine nodule. Geochimica et Cosmochimica Acta, 68(14): 3125–3136, doi: 10.1016/j.gca.2004.01.015
Maréchal C N, Nicolas E, Douchet C, et al. 2000. Abundance of zinc isotopes as a marine biogeochemical tracer. Geochemistry, Geophysics, Geosystems, 1(5): 1015
Maréchal C N, Télouk P, Albarède F. 1999. Precise analysis of copper and zinc isotopic compositions by plasma-source mass spectrometry. Chemical Geology, 156(1–4): 251–273, doi: 10.1016/S0009-2541(98)00191-0
Mason T F D, Weiss D J, Chapman J B, et al. 2005. Zn and Cu isotopic variability in the Alexandrinka volcanic-hosted massive sulphide (VHMS) ore deposit, Urals, Russia. Chemical Geology, 221(3–4): 170–187, doi: 10.1016/j.chemgeo.2005.04.011
Mason T F D, Weiss D J, Horstwood M, et al. 2004. High-precision Cu and Zn isotope analysis by plasma source mass spectrometry Part 1: Spectral interferences and their correction. Journal of Analytical Atomic Spectrometry, 19: 209–217, doi: 10.1039/b306958c
McManus J, Berelson W M, Severmann S, et al. 2006. Molybdenum and uranium geochemistry in continental margin sediments: Paleoproxy potential. Geochimica et Cosmochimica Acta, 70(18): 4643–4662, doi: 10.1016/j.gca.2006.06.1564
Moeller K, Schoenberg R, Pedersen R B, et al. 2012. Calibration of the new certified reference materials ERM-AE633 and ERM-AE647 for Copper and IRMM-3702 for zinc isotope amount ratio determinations. Geostandards and Geoanalytical Research, 36(2): 177–199, doi: 10.1111/j.1751-908X.2011.00153.x
Moffett J W, Dupont C. 2007. Cu complexation by organic ligands in the sub-arctic NW Pacific and Bering Sea. Deep-Sea Research Part I: Oceanographic Research Papers, 54(4): 586–595, doi: 10.1016/j.dsr.2006.12.013
Morel F M M, Price N M. 2003. The biogeochemical cycles of trace metals in the oceans. Science, 300(5621): 944–947, doi: 10.1126/science.1083545
Nägler T F, Neubert N, Böttcher M E, et al. 2011. Molybdenum isotope fractionation in pelagic euxinia: Evidence from the modern Black and Baltic Seas. Chemical Geology, 289(1–2): 1–11, doi: 10.1016/j.chemgeo.2011.07.001
Navarrete J U, Borrok D M, Viveros M, et al. 2011. Copper isotope fractionation during surface adsorption and intracellular incorporation by bacteria. Geochimica et Cosmochimica Acta, 75(3): 784–799, doi: 10.1016/j.gca.2010.11.011
Pasquarello A, Petri I, Salmon P S, et al. 2001. First solvation shell of the Cu(II) aqua ion: evidence for fivefold coordination. Science, 291(5505): 856–859, doi: 10.1126/science.291.5505.856
Peacock C L, Sherman D M. 2007. Crystal-chemistry of Ni in marine ferromanganese crusts and nodules. American Mineralogist, 92(7): 1087–1092, doi: 10.2138/am.2007.2378
Pichat S, Douchet C, Albarède F. 2003. Zinc isotope variations in deep-sea carbonates from the eastern equatorial Pacific over the last 175 ka. Earth and Planetary Science Letters, 210(1–2): 167–178, doi: 10.1016/S0012-821X(03)00106-7
Piper D Z, Williamson M E. 1977. Composition of Pacific Ocean ferromanganese nodules. Marine Geology, 23(4): 285–303, doi: 10.1016/0025-3227(77)90036-6
Poulson Brucker R L, McManus J, Severmann S, et al. 2009. Molybdenum behavior during early diagenesis: Insights from Mo isotopes. Geochemistry, Geophysics, Geosystems, 10(6): Q06010
Poulson R L, Siebert C, McManus J, et al. 2006. Authigenic molybdenum isotope signatures in marine sediments. Geology, 34(8): 617–620, doi: 10.1130/G22485.1
Schauble E A. 2004. Applying stable isotope fractionation theory to new systems. Reviews in Mineralogy & Geochemistry, 55(1): 65–111
Scott C, Lyons T W. 2012. Contrasting molybdenum cycling and isotopic properties in euxinic versus non-euxinic sediments and sedimentary rocks: Refining the paleoproxies. Chemical Geology, 324–325: 19–27, doi: 10.1016/j.chemgeo.2012.05.012
Siebert C, McManus J, Bice A, et al. 2006. Molybdenum isotope signatures in continental margin marine sediments. Earth and Planetary Science Letters, 241(3–4): 723–733, doi: 10.1016/j.epsl.2005.11.010
Takano S, Tanimizu M, Hirata T, et al. 2014. Isotopic constraints on biogeochemical cycling of copper in the ocean. Nature Communications, 5(1): 5663, doi: 10.1038/ncomms6663
Thompson C M, Ellwood M J. 2014. Dissolved copper isotope biogeochemistry in the Tasman Sea, SW Pacific Ocean. Marine Chemistry, 165: 1–9, doi: 10.1016/j.marchem.2014.06.009
Thompson C M, Ellwood M J, Wille M. 2013. A solvent extraction technique for the isotopic measurement of dissolved copper in seawater. Analytica Chimica Acta, 775: 106–113, doi: 10.1016/j.aca.2013.03.020
Valley J W, Cole D R. 2001. Reviews in Mineralogy and Geochemistry Volume 43: Stable Isotope Geochemistry. Washington, DC: Mineralogical Society of America, 87–94
Vance D, Archer C, Bermin J, et al. 2008. The copper isotope geochemistry of rivers and the oceans. Earth and Planetary Science Letters, 274(1–2): 204–213, doi: 10.1016/j.epsl.2008.07.026
Vance D, Zhao Y, Cullen J, et al. 2012. Zinc isotopic data from the NE Pacific reveals shallow recycling. Mineral Mag, 76: 1486